Environmental Research 171 (2019) 1–10

Contents lists available at ScienceDirect

Environmental Research

journal homepage: www.elsevier.com/locate/envres

How graphene affects the misfolding of human prion protein: A combined experimental and molecular dynamics simulation study

Yongchang Zhu[a], Jingjing Guo[a], Ai Zhang[a], Lanlan Li[b], Xuewei Liu[a], Huanxiang Liu[a,b,*], Xiaojun Yao[b,c,*]

[a] School of Pharmacy, Lanzhou University, Lanzhou 730000, China
[b] State Key Laboratory of Applied Organic Chemistry and Department of Chemistry, Lanzhou University, Lanzhou 730000, China
[c] State Key Laboratory of Quality Research in Chinese Medicine, Macau Institute for Applied Research in Medicine and Health, Macau University of Science and Technology, Taipa, Macau, China

ARTICLE INFO

Keywords:
Graphene
Prion
Molecular dynamics simulation
Conformational change
Misfolding

ABSTRACT

As the broad application of graphene in the biomedical field, it is urgent and important to evaluate how the graphene affects the structure and function of the proteins in our body, especially the amyloid-related proteins. Prion protein, as a typical amyloid protein, it misfolding and aggregation will lead to serious prion diseases. To explore if graphene promotes or inhibits the formation of amyloid, here, we combined the experimental and molecular dynamics (MD) simulation methods to study the influence of graphene on the globular domain of prion protein ($PrP_{117–231}$). The results from fluorescence quenching and circular dichroism spectrum showed that the addition of graphene changed the secondary structure of prion protein largely, mainly reflecting in the reduced α-helix structure and the increased coil structure, indicating graphene may strengthen the misfolding inclination of prion. To further uncover the mechanism of conformational change of prion under the induction of graphene, the all-atoms MD simulations in explicit solvent were performed. Our simulations suggest that prion protein can be quickly and tightly adsorbed onto graphene together with the weak conformational rearrangement and may reorient when approaching the surface. The Van der Waals' force drive the adsorption process. In the induction of graphene, H1 and S2-H2 loop regions of prion become unstable and prion begins to misfold partially. Our work shows that graphene can induce the misfolding of prion protein and may cause the potential risk to biosystems.

1. Introduction

Since its discovery in 2004, graphene has attracted great attention from various fields, due to its remarkable electrical, optical, physical and chemical properties. Until 2008, the potential biomedical applications of graphene started to attract the attention of scientists, including drug/gene delivery, biosensing, bioimaging, antibacterial materials, biocompatible scaffold for cell culture, and so on (Brannon-Peppas and Blanchette, 2004; Feng and Liu, 2011; Gurunathan and Kim, 2016; Jarosz et al., 2016; Mendes et al., 2013; Shen et al., 2012; Zhang et al., 2012). As we know, when nanoparticles (NPs) enter a biological medium, proteins and other biomolecules rapidly compete for binding to the NP surface either strongly or weakly, leading to the formation of a dynamic protein corona (Ashby et al., 2014; Cedervall et al., 2007; Mahmoudi et al., 2011; Tenzer et al., 2011). Their interaction with proteins can cause the perturbation of both protein structure and function. When NPs interact with biological enzymes, they may cause the enzymes to loss their original conformations and inhibit or improve the functions of the enzymes (Chen et al., 2017; Merli et al., 2011). For example, as reported by Chen et al. (2017), when SWCNTs interact with lignin peroxidase and maleylpyruvate isomerase, the functions of the enzymes were inhibited. In addition, the interaction between NPs and amyloid proteins or peptides might inhibit or facilitate amyloid formation (Bobylev et al., 2010; Dominguez-Medina et al., 2016; Fei and Perrett, 2009; Guo et al., 2013; Kim and Lee, 2003; Kowalewski and Holtzman, 1999; Lee et al., 2011; Li et al., 2011; Linse et al., 2007; Mahmoudi et al., 2012; Podlubnaya et al., 2006). Owing to high specific surface area, graphene-family nanomaterials possess potentially larger protein adsorption capacities than most other nanomaterials (Bianco et al., 2008; Sanchez et al., 2011). In spite of growing number of computational studies dealing with the interaction between graphene and proteins, little is known about the

* Corresponding authors at: State Key Laboratory of Applied Organic Chemistry and Department of Chemistry, Lanzhou University, Lanzhou 730000, China.
E-mail address: hxliu@lzu.edu.cn (H. Liu).

https://doi.org/10.1016/j.envres.2018.12.057
Received 19 August 2018; Received in revised form 15 December 2018; Accepted 23 December 2018
Available online 28 December 2018
0013-9351/

effects of graphene on the structure of amyloidosis protein. Thus, whether graphene inhibits or promotes amyloid formation is still a controversial issue. Therefore, one critical issue to be resolved before further applications of graphene in biomedicine is the potential short- and long-term toxicity of this new nanomaterial (Baldrighi et al., 2016; de Luna et al., 2016; Elsaesser and Howard, 2012; Sharifi et al., 2012).

Here, to uncover the effects of graphene on amyloid-related proteins, we combined the experimental and molecular dynamics (MD) simulation methods to study the influence of graphene on the globular domain of normal cellular prion protein (PrP^C). The misfolding and aggregation of prion protein will lead to the serious prion diseases and it is also the key factor for the development of early diagnosis and highly sensitive detection technologies of PrP related biomolecules (Zhang et al., 2011; Lou et al., 2017a, 2017b; Kouassi et al., 2007; Liang et al., 2013; Lou et al., 2017a, 2017b). Prion diseases (Chen and Dong, 2016; de Luna et al., 2016) are the only known infectious amyloid diseases. The conversion of prion protein (PrP) from its cellular form (PrP^C) to its pathogenic form (PrP^{Sc})(Prusiner et al., 1983) is the key procedure of development of prion diseases. The globular domain of normal cellular prion protein (PrP^C) is rich in the α-helix structure. Once the misfolding happens, it will be transitioned to the structure rich in β-sheet (Lou et al., 2015; Sun et al., 2015; Wang et al., 2015). Here, to monitor if the prion protein will misfold induced by graphene, fluorescence quenching method and circular dichroism (CD) spectra were used. Although these experimental methods can give us the direct evaluation if the secondary structure of prion protein will change or not, they can't give the mechanism of structure transition. Thus, to explore how prion protein interact with graphene and uncover the structure transition of prion protein, the molecular dynamics (MD) simulation was performed. Compared to the experimental method, MD simulation can provide more detailed and dynamic interaction information between protein and nanoparticles. Additionally, the induced structural change of protein by graphene can be also observed easily by analyzing the MD simulation trajectory.

2. Materials and methods

2.1. Cloning, expression and purification of $Prion_{117–231}$

The genes of prion protein ($PrP_{117–231}$) were synthesized by GENEWIZ, Inc. Suzhou, China and were cloned into the pET-28b derived plasmid containing 6 × His tag. The plasmid was transformed into *Escherichia coli* strain BL21 (DE3) (Conway et al., 1998) competent cells by heat-shock at 42 °C for 60 s. The prion proteins ($PrP_{117–231}$) were expressed and purified as described (Li et al., 2017). The purity and concentration of the refolded protein were determined using a 12% SDS-PAGE and a Nanodrop 2000 equipment, respectively. Finally, the protein was stored lyophilized at −80 °C.

2.2. Fluorescence quenching measurements

All fluorescence spectra were recorded on a Perkin-Elmer LS 55 Fluorescence Spectrometer. The excitation wavelength at 285 nm was used to selectively excite tryptophan residues and the emission spectra was monitored in the range of 300–500 nm with a fixed slit width of 5 nm. After diluting with 10 mM Tris-HCl, 10 μM $PrP_{117–231}$ was selected and added to different concentrations of graphene (0.04 mg/ml, 0.05 mg/ml, 0.06 mg/ml, 0.07 mg/ml, 0.08 mg/ml, 0.09 mg/ml, 0.10 mg/ml). The suspended solution was used for depicting fluorescence intensity curves.

2.3. CD spectroscopy

Circular dichroism (CD) spectra were recorded on OLIS-052711-DSM1000, which was a CD spectropolarimeter with a 5 mm sample cell and the scan wavelengths ranged from 190 nm to 240 nm. Various concentrations of graphene (0.4 mg/ml, 0.6 mg/ml, 0.8 mg/ml, 1.0 mg/ml, 1.2 mg/ml) were mixed with 20 μM $PrP_{117–231}$ and then subjected to the measurement at room temperature. The ellipticity [θ] (degrees) or differential absorbance (Δ*A*) is used to describe the CD data. The mean residue ellipticity ($[\theta]_{mrw,\lambda}$) at wavelength λ is given by:

$$[\theta]_{mrw,\lambda} = \frac{\theta_\lambda}{10} \cdot \frac{MRW}{c \cdot l} \quad (1)$$

where θ_λ is the observed ellipticity (degrees) at the wavelength λ , *l* is the pathlength (cm), and *c* is the concentration (g/ml). The Mean Residue Weight (MRW) is calculated from $MRW = M/(N-1)$, where M is the total molecular mass of the protein, and N is the number of amino acids.

And $\Delta\varepsilon$ (the molar differential extinction coefficient) is a good check on the protein structure characteristics at a certain wavelength. There is a close relationship between $[\theta]_{mrw}$ and $\Delta\varepsilon$ (Kelly et al., 2005):

$$[\theta]_{mrw} = 3298 \times \Delta\varepsilon \quad (2)$$

The units of $\Delta\varepsilon$ are $M^{-1}\ cm^{-1}$. The final results were analyzed using SELCON3 software (Calzolai and Zahn, 2003b).

2.4. Molecular dynamics simulations

2.4.1. The construction of simulation system

The 3D structure of human PrP was retrieved from the PDB database (https://www.rcsb.org, PDB ID: 1HJN) obtained by NMR at pH 7.0 (Calzolai and Zahn, 2003a), which contains the C-terminal globular domain of PrP consisting of residues 125–228. The globular domain contains three α-helices (H1, H2, H3) and two very short anti-parallel β-sheets (S1, S2) (Donne et al., 1997; Riek et al., 1996). The graphene sheet with the size 65 Å × 65 Å is used in this study, which is large enough for the prion protein. The adsorption of proteins on the graphene may depend on the initial orientation of the proteins relative to the surface, but significant peptide rotation was generally prevented by all-atom explicit-solvent MD simulation within nanosecond time scale. In our simulations, to ensure the enough interaction between graphene and prion, three initial orientations of prion protein were selected by keeping the long axis parallel to the graphene surface with the three typical faces facing graphene (shown in Fig. 1): 1) the H2 helix and the C-terminal of H1; 2) the beta-sheet and the N-terminals of the three helices (H1, H2 and H3); 3) H1 and the C-terminals of H2 and H3. Therefore, based on the three constructs, every part of PrP has a large probability to contact with graphene. In the initial complexes, the minimum distance between graphene and prion was set at least 5 Å, allowing PrP to freely rotate and adjust its orientation and to reduce the diffusion time approaching the graphene surface.

2.4.2. Molecular dynamics simulations in explicit solvent

We performed MD simulations with TIP3P (Jorgensen et al., 1983) waters using AMBER 10 software package (Case et al., 2008) and AMBER ff03 (Duan et al., 2003; Lee and Duan, 2004) force field since previous MD simulation studies have shown that AMBER ff03 can reproduce the secondary structures of peptides comparable to experimental measurements when the peptides are adsorbed on carbon nanotube or graphene (Balamurugan et al., 2010). Na^+ ions were added to keep the systems neutral. The complexes and the isolated protein were placed in a rectangular box and truncated octahedral box, respectively. The distance between protein/graphene and box-boundary was set at least 11 Å. To reduce the solvent boxes, several carbon atoms of four corners in the graphene sheet were deleted here. The total atom numbers of three systems with graphene are 40663, 43189, 44287, respectively. Firstly, we used steepest decent method and conjugate gradient method to minimize each system. Subsequently, the systems were heated up from 0 to 310 K with a force weight of 2.0 kcal/(mol $Å^2$) on the graphene. All bond lengths involving hydrogens were constrained using the SHAKE algorithm (Ryckaert et al., 1977), 2-fs time

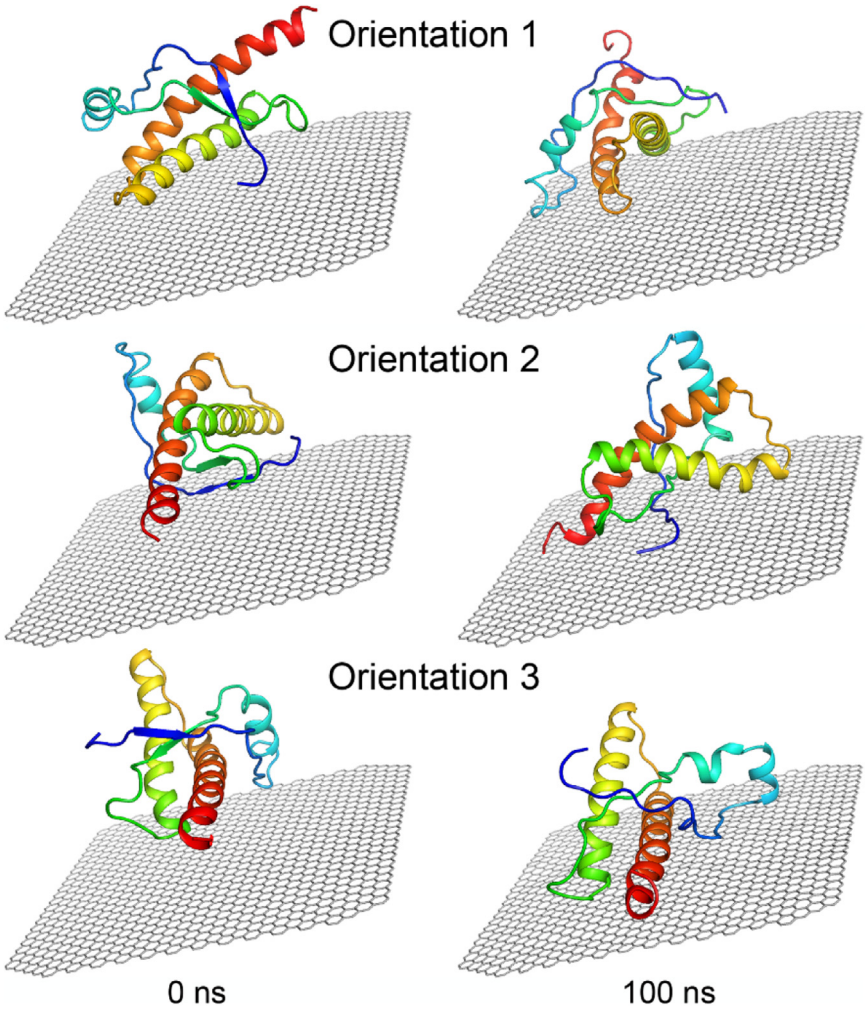

Fig. 1. The structures of prion protein above the graphene surface before and after 100 ns simulation. The protein was shown as cartoon colored from blue (the N-terminus) to red (the C-terminus) and the graphene was shown as sticks in gray. (For interpretation of the references to color in this figure legend, the reader is referred to the web version of this article.)

step was made use of integrating the equations of motion. The non-bonded cutoff distance was 10 Å and the long-range electrostatics interactions were calculated by using the Particle Mesh Ewald(PME) (Essmann et al., 1995) method. The Langevin thermostat was used to regulate the temperature of the system. All equilibration and subsequent MD stages were carried out in the isothermal isobaric (NPT) ensemble using a Berendsen barostat (Berendsen et al., 1984). There were no restrains on protein but a force constant of 2.0 kcal/mol Å^2 on graphene. Each complex system was simulated for 100 ns to investigate the initial adsorption stage. Neutral pH and physiological temperature (310 K) are controlled in all simulations.

2.5. Trajectory analysis methods

The trajectories were analyzed using AMBER 10 (Case et al., 2008) and VMD (Humphrey et al., 1996) programs. To evaluate the compactness of the studied protein, the size of protein was roughly estimated by radius of gyration (Rg), which is defined as the mass-weighted positional mean of the distances of atoms from the center of mass. Here, Rg was calculated for CA atoms of the whole protein and the hydrophobic core, respectively. The secondary structures were assigned using the dictionary of secondary structure of proteins (DSSP) program developed by Kabsch and Sander (1983).

The interface area or contact area is the area of the molecular surface buried in contact surface between the two molecules. It was calculated as below (Balamurugan et al., 2011):

$$Contact\ Area = \frac{1}{2}\left[(SAS_{pep} + SAS_{gra}) - SAS_{complex}\right]$$

Here, SAS_{gra} and SAS_{pep} are solvent accessible surface area of the isolated graphene and prion, respectively, and SAS_{complex} is that of the graphene-prion complex.

To investigate the binding affinity between prion protein and graphene, Molecular Mechanics/Generalized Born Surface Area (MM-GBSA), which has been successfully applied in free energy calculations (Hou et al., 2011a), were applied. For each snapshot extracted from the last 15 ns MD simulation, the free energy is calculated for each molecular species (complex, protein, and graphene), and the binding free energy is computed by using the following formula:

$$\Delta G_{bind} = G_{complex} - G_{protein} - G_{graphene}$$

The free energy, G, for each species can be calculated by the following scheme using the MM-GBSA methods: (Kollman et al., 2000; Srinivasan et al., 1998)

$$G = E_{gas} + G_{sol} - TS$$

$$E_{gas} = E_{int} + E_{vdW} + E_{ele}$$

$$G_{polar} = E_{ele} + G_{sol\_polar}$$

$$G_{sol} = G_{sol\_polar} + G_{sol\_np}$$

$$G_{sol\_np} = \gamma SAS$$

where, E_{gas} is the gas-phase energy; E_{int} is the internal energy; E_{ele} and E_{vdw} are the Coulomb and van der Waals energies, respectively. G_{sol} is the solvation free energy and can be decomposed into polar and nonpolar contributions. G_{sol_polar} is the polar solvation contribution calculated by solving GB equation. G_{sol_np} is the nonpolar solvation contribution and was estimated by the solvent accessible surface area (SAS) determined using a water probe radius of 1.4 Å. In MM-GBSA calculation, the solute dielectric constant (ε_{in}) is a key parameter for the calculation of electrostatic energy. By considering the polarity of the studied protein and the results of reference, (Hou et al., 2011a; Hou et al., 2011b) here, we set the solute dielectric constant as 2.0. T and S are the temperature and the total conformational entropy of protein, respectively. The normal-mode analysis was performed here to evaluate the conformational entropy change (-TΔS) using the nmode program in AMBER 10.0. (Case et al., 2008), in which the entropy term is divided into the contribution of translational, rotational, and vibrational entropies.

Using the GB model, it was possible to compute the binding free energy contribution of each residue at the interface between two interacting molecules. The contribution of a given residue can be obtained by summing the contribution of each atom of the residue. To obtain a detailed view of the interaction between graphene and proteins, the binding free energy decomposition was performed using MM-GBSA method.

3. Results and discussion

3.1. The interaction between graphene and $PrP_{117–231}$

In the presence of different concentrations of graphene, the fluorescence spectra of $PrP_{117–231}$ were collected and displayed in Fig. 2. Here, the "blank-line" is the fluorescence intensity of $PrP_{117–231}$ without graphene. As the concentration of graphene increased, the fluorescence intensity of protein decreased, indicating that graphene could quench the intrinsic fluorescence of prion in a concentration dependent manner. Particularly, when the concentration of graphene was up to 0.10 mg/ml, the fluorescence intensity reduced by half. The strong quenching of fluorescence indicates that the conformation of aromatic amino acids significantly changed under the influence of graphene. To further identify the detailed changes in secondary structure of $PrP_{117–231}$, circular dichroism analysis was performed.

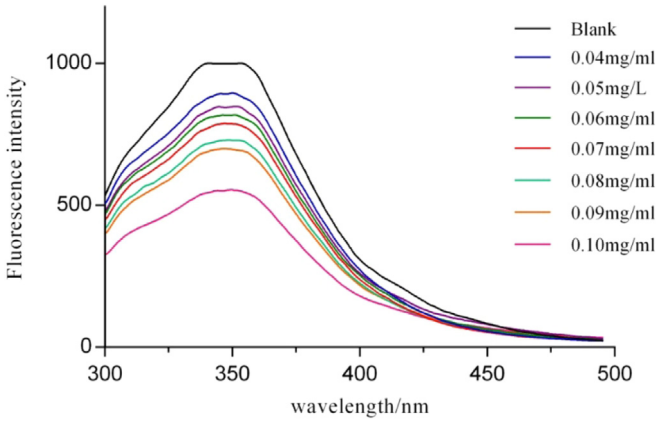

Fig. 2. Fluorescence spectra of the PrP117–231 at different concentrations of graphene.

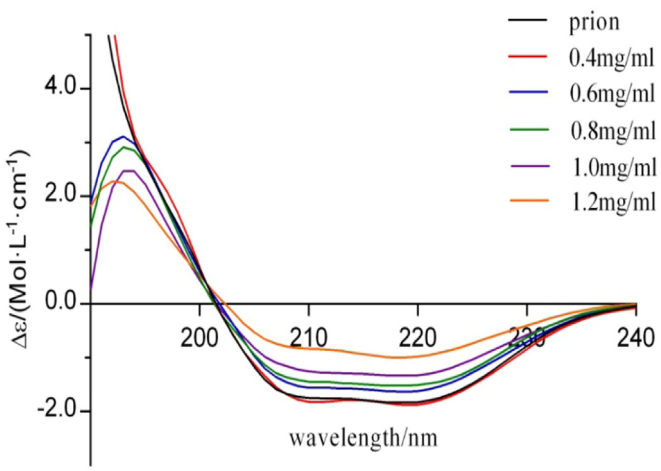

Fig. 3. CD spectra of the PrP117–231 at different concentrations of graphene. "Prion" is the blank system without graphene.

3.2. The secondary structure changes of $PrP_{117–231}$ induced by graphene

CD can be used to determine the secondary structural content of interested proteins. The negative peaks appearing at 208 and 222 nm and the positive peak appearing at 192 nm (Matsuo et al., 2012) in CD spectra are the characteristics of α-helical structure of proteins while the negative peak appearing at 215 nm (Matsuo et al., 2012) and the positive peak appearing at 195 nm are the characteristics of β-sheet structure. Any variation in these bands is related with a conformational change of protein. Based on CD spectra, the secondary structure contents of $PrP_{117–231}$ were calculated. With the concentration of graphene increasing, the peak intensities at 208, 222 and 192 nm decreased, indicating that the amount of α-helical structure decreased (Fig. 3).

In order to further accurately calculate the secondary structure contents of PrP117–231, the data were analyzed using the SELCON3 program (Matsuo et al., 2016) and the results were listed in Table 1. The main secondary structure of prion without graphene was α-helix with the content of 72.8%, while the β-sheet and turn were 2.4% and 4.6%, respectively. When the concentration of graphene is 0.4 mg/ml, the secondary structure of prion has no obvious change, indicating that in the low concentration of graphene, the structure of prion wasn't perturbed. But when the concentration of graphene is higher than 0.6 mg/ml, the secondary structure of prion will change largely. From the Table 1, it can be seen that the content of β-sheet increased and the content of α-helix decreased when the concentration of graphene is higher than 0.6 mg/ml, indicating that graphene with the certain concentration can induce the misfolding of prion partially.

3.3. Dynamical adsorption of PrP125–228 on the graphene surface

To explore the mechanism of structural transformation of prion induced by graphene, the MD simulations were performed in explicit

Table 1
The secondary structure contents of $PrP_{117–231}$ at different concentrations of graphene obtained by CD spectra.

The concentrations of graphene	Secondary structure content (%)				
	α-helix	Beta-sheet	Turn	Coil	Sum
0.0 mg/ml	72.8	2.40	4.60	22.5	102.4
0.4 mg/ml	80.4	0.30	5.30	15.2	101.1
0.6 mg/ml	43.1	8.20	20.4	28.7	100.5
0.8 mg/ml	36.3	7.00	22.6	30.7	100.2
1.0 mg/ml	46.3	12.9	15.0	23.7	97.8
1.2 mg/ml	40.7	14.7	15.7	26.8	98.0

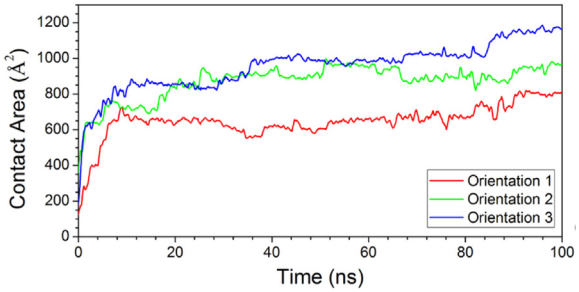

Fig. 4. The contact area between graphene and PrP as a function of simulation time averaged over 500 ps.

solvent. For the all-atom MD simulations, the contact area between the atoms of graphene and $PrP_{125–228}$ was monitored as a function of simulation time to show the dynamic interactions between graphene and PrP. It can be seen from Fig. 4 that at the first 10 ns the contact areas are keeping a good upward trend and reached equilibrium in the last 10 ns with the contact number in a relatively high level. Although the different orientations (Fig. 1) lead to varying degrees of the contact area, the relative high values indicate PrP can form good contacts with graphene. Therefore, the adsorption process is very quick and the interaction between graphene and the protein is very stable in all orientations.

3.4. The structural changes of prion upon the adsorption on graphene

To explore if the adsorption of PrP on graphene surface will affect its structural features, the structural changes of prion during the molecular dynamics simulation were analyzed further. Firstly, the root-mean-square fluctuations (RMSFs) of Cα atoms of prion were calculated. As shown in Fig. 5, the Cα RMSFs show similar manners for all runs. For the residues (174–188 and 202–220) of core domain, the RMSFs values are rather small in the adsorption runs and the reference run, further showing the corresponding H2 and H3 regions are very stable, which is in well agreement with our previous work (Guo et al., 2012a; Guo et al., 2012b). Relative to H2 and H3 region, the H1 region is more flexible in all systems, which is also verified in previous study (Zhou et al., 2017). H1 is unstable and easy to misfold. Additionally, two ends and the loop regions are also very flexible.

Compared with the isolated PrP, the RMSF values of many residues in the adsorption runs increased, especially residues 133–140 (S1-H1 loop), 149–161 (H1 and H1-S2 loop), 192–200 (H2-H3 loop), and residues 209–218 (the middle part of H3) in Orientation 1 and 3, indicating that the flexibility of PrP in the two runs increased after adsorption on graphene surface. The residues in Orientation 2 have the smallest structural fluctuation, suggesting although this orientation has more contacts with graphene than Orientation 1, the adsorption has a very small influence on the protein flexibility after the 100-ns simulation.

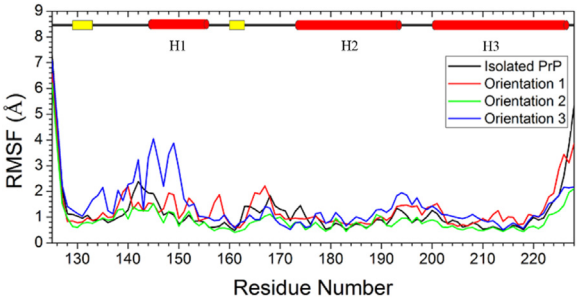

Fig. 5. The RMSFs of Cα atoms as a function of residue number for the last 25 ns simulations.

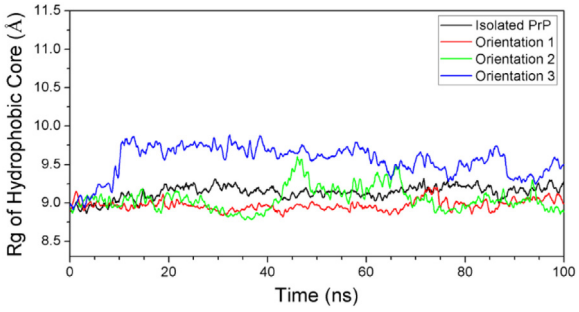

Fig. 6. Radius of gyration for the hydrophobic core of PrP as a function of simulation time for all systems averaged over 500 ps.

By comparing the simulation results starting from different orientations of prion protein relative to graphene, we speculate two possible adsorption processes can occur. One is the initial adsorption of a protein on graphene is accompanied by significant conformational changes of some “soft” local regions in contact with the surface, such as H1 of PrP in Orientations 1 and 3. The other one is preserving the native stable secondary structures and the overall globular shape at the beginning of adsorption process (i.e. Orientation 2). In Orientation 2, one β-strand (S2) is adhered to the graphene surface without significant conformational changes due to its intrinsic flat structure, while the N-terminal of H1 and the C-terminal of H2 start to lose their initial helical structures. Hence, much larger rearrangements might take place at longer times during the MD runs, eventually yielding similar adsorption conformation.

To evaluate the stability of the globular domain of PrP, generally, a core of hydrophobic side chains is defined in the prion protein, which contains residues 134, 137, 139, 141, 158, 161, 175, 176, 179, 180, 184, 198, 203, 205, 206, 209, 210, and 213–216. In order to measure its compactness during the simulations, we monitored Rg of the CA atoms of the hydrophobic core, and the results are shown in Fig. 6.

In Fig. 6, it can be seen that the Rg values in the isolated run maintain around 9.25 Å and have a narrow fluctuation margin during all 100 ns simulation. However, the Rg values in the adsorption runs have obvious dramatic fluctuations. At the end of the simulations, it can be seen that except for Orientation 3, the adsorption made the PrP (125–228) more compact than the isolated protein. With the interaction between graphene and protein, PrP may experience a structural transition progress during adsorption. In order to show the structural transition progress, we calculated the average CA-CA distances for PrP (125–228) in all runs. To show the movement of each residue more clearly, only relative change of the CA-CA distance between the isolated run and the adsorption runs are shown in Fig. 7. In this figure, different colors indicate different changes in the CA-CA distance. For example, blue represents the adsorption makes the distance shorter, while red represents the adsorption makes the distance longer. The distance changes mainly locate at the first helix (H1) region in all adsorption simulations. For Orientation 1 and 2, the H1 of PrP becomes closer to S2-H2 and H3, while for Orientation 3 it is on the contrary. Apparently, Orientation 2 with the smallest color range has the weakest structural changes, which agrees with the RMSF results. Although Orientation 1 and 3 have obvious fluctuations in the structure of protein, the changes of their CA-CA distances are opposite. In Orientation 3, H1 moves away from H2 and H3, leading to the high Rg values, while in Orientation 1 and 2, H1 becomes closer to H2 and H3. Although there are different movement trend of H1 in different orientation, the common feature is that H1 is becoming unstable in the induction of graphene.

To further explore the detailed structural changes of PrP during adsorption, the analysis of the secondary structures were performed. The secondary structure information for each residue (residues 125–228) during the simulations was given in Fig. 8. It can be seen that the secondary structures have no obvious changes during the isolated

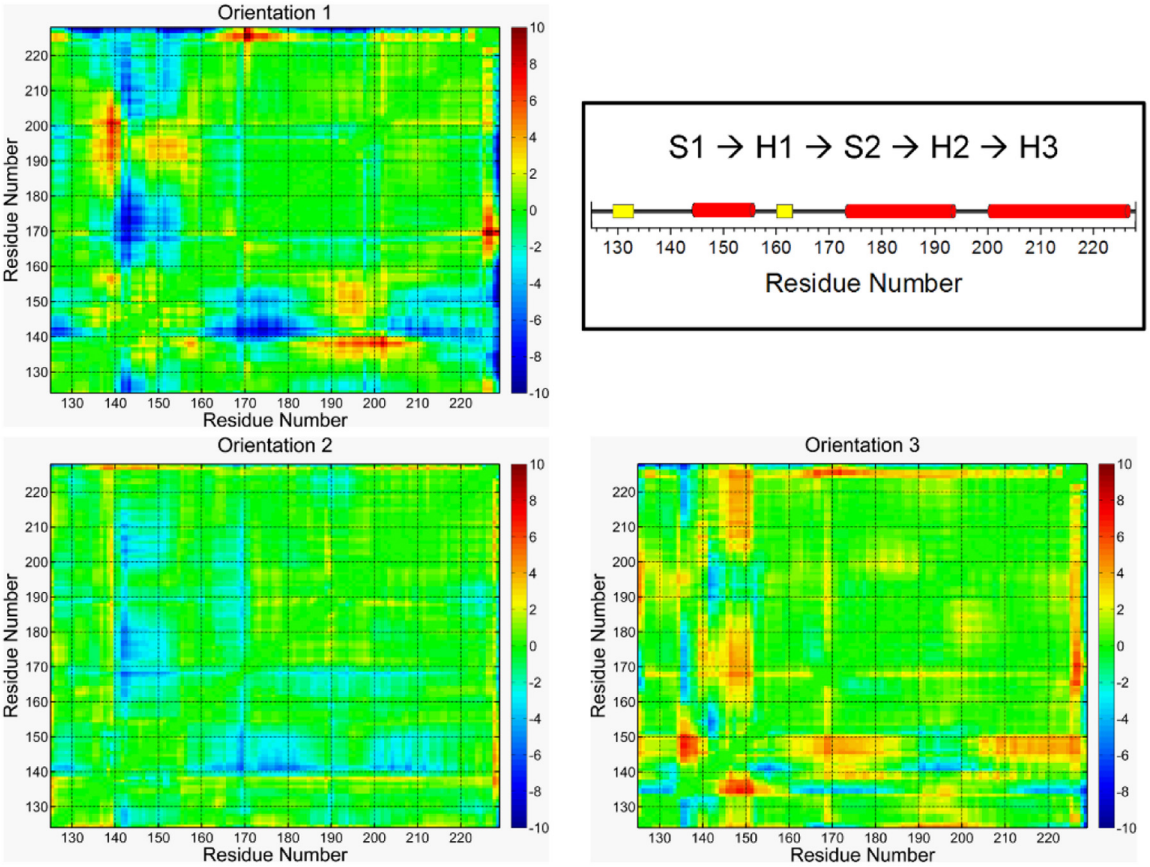

Fig. 7. The difference of the average CA-CA distance (Å) between the isolated run and the adsorption runs during the last 25 ns ($\Delta Dist = Dist_{adsorption}$-$Dist_{isolated}$).

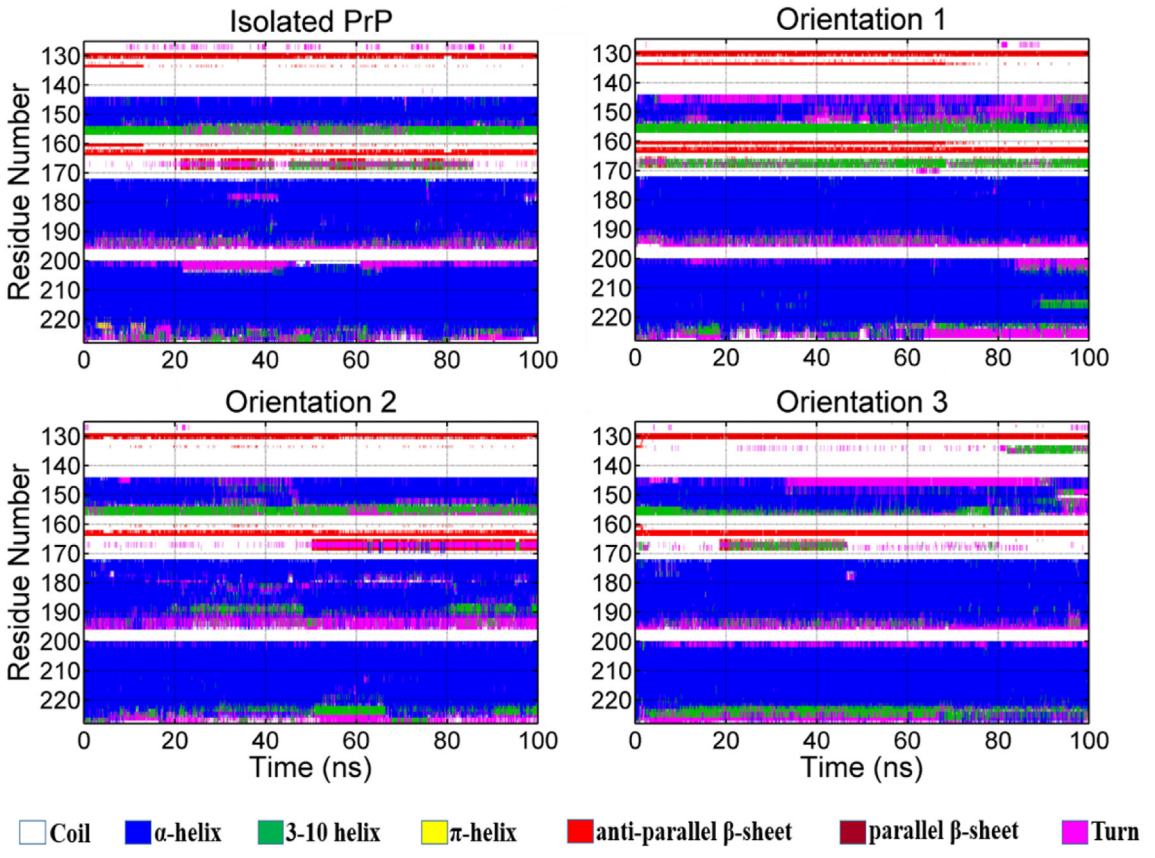

Fig. 8. Secondary structure analysis for PrP simulated in explicit solvent.

Table 2
The averaged secondary structure contents of prion protein in the last 10 ns simulation.

System	Secondary structure content (%)						
	α-helix	3_{10}-helix	π-helix	Helix	Sheet	Turn	Coil
Isolated PrP	50.84 ± 2.88	4.28 ± 1.77	0.11 ± 0.60	55.22 ± 2.60	3.85 ± 0.32	5.82 ± 2.51	35.10 ± 1.47
Orientation 1	40.51 ± 3.60	10.24 ± 3.05	0.00 ± 0.08	50.76 ± 3.51	3.93 ± 0.48	12.94 ± 3.34	32.37 ± 0.95
Orientation 2	46.14 ± 3.10	6.72 ± 2.65	0.01 ± 0.19	52.88 ± 2.87	5.36 ± 0.91	10.38 ± 2.93	31.39 ± 1.50
Orientation 3	47.59 ± 4.45	6.27 ± 3.12	0.05 ± 0.38	53.90 ± 4.65	3.83 ± 0.26	10.16 ± 4.29	32.10 ± 1.23

simulation, indicating that the wild type PrP is rather stable. Nevertheless, the secondary structures of PrP in adsorption simulations change more obviously. In Orientation 1, the H1 region is instable, and the S2-H2 loop forms a 3_{10}-helix. In Orientation 2, the H2 region is not stable during the simulation, especially at residue 180 and the tail of H2. The H1 region is also very flexible in Orientation 3, particularly at the end of simulation. These results indicate that the prion protein experiences the structural transitions during the adsorption on graphene.

As can be seen in Table 2, the β-sheet contents were maintained at almost the same level in the absence and presence of graphene, while the α-helical contents decreased slightly and turn contents increased in the adsorption simulations compared with that in the isolated PrP simulation, which is consistent with the results of CD spectra. The 3_{10}-helical contents in adsorption runs, especially in Orientation 1, are larger than that in the isolated simulation. From Fig. 8, it can be seen that H1 region and the tail of H2 and H3 are responsible for the decreasing of α-helical content. Whatever, the α-helical content decreased and the 3_{10}-helical and turn contents increased after adsorption on graphene surface, which is a critical feature in the misfolding progress of PrP.

Previous studies showed that the S2-H2 loop is important for the template-driven amplification of prion (Kaneko et al., 1997), and behaves as a motif with self-assembly properties (Christen et al., 2009). As Fig. 8 shows, in MD simulation of the adsorbed prion in Orientation 1, the conformational transition of the S2-H2 loop to a 3_{10} helix was observed, which is consistent with the previous reports (Guo et al., 2012a; Meli et al., 2011). This result suggests the S2-H2 loop undergoes a structural rearrangement during the adsorption progress.

The above result suggests that graphene may induce the misfolding of prion by making H1 unfold and S2-H2 loop transition to 3_{10} helix. Although the initial orientation determines which parts of protein will contact with graphene at first, and be affected mostly, it is obvious that the adsorption indeed induces the conformational changes in all orientations.

3.5. The driving force of the interaction between prion and graphene

For a protein to adsorb to a surface, it must first contact and "stick" at that surface. The affinity of a protein with a surface depends on several factors, including both the nature of the adsorbent surface and the surface of the protein that first contacts the adsorbent surface. Several simulation studies have demonstrated the importance of the orientation of protein (or protein-like) molecules on their adsorption at surfaces (Mücksch and Urbassek, 2011; Wei et al., 2012; Yu et al., 2012; Zhou et al., 2004). Here, to further identify the driving force of the adsorption process, MM-GBSA calculations were performed. The results of free energy calculations were shown in Table 3. It can be seen that graphene has a strong adsorption capacity to the globular domain of prion protein, with binding affinities larger than 100 kcal mol^{-1}. The binding free energies for adsorption runs are −104.80 (Orientation 1), −150.62 (Orientation 2), and −177.09 (Orientation 3) kcal mol^{-1}, respectively, indicating different orientations result in the different binding affinities between protein and graphene. Therefore, we denote the weak physisorption attraction pulls the protein toward the surface

Table 3
The components and standard errors of binding free energy for prion protein adsorbing on graphene. (kcal mol^{-1}).

Contribution	Orientation 1		Orientation 2		Orientation 3	
	Average	Std[a]	Average	Std[a]	Average	Std[a]
ΔE_{ele}	0.00	0.00	0.00	0.00	0.00	0.00
ΔE_{vdw}	−154.75	13.77	−190.25	9.49	−237.40	12.86
ΔE_{int}	−0.00	0.00	0.00	0.00	0.00	0.00
ΔE_{gas}	−154.75	13.77	−190.25	9.49	−237.40	12.86
ΔG_{sol_np}	−12.85	1.01	−15.41	0.59	−18.33	1.08
ΔG_{sol_polar}	26.60	2.12	15.10	0.76	34.30	2.36
ΔG_{sol}	13.75	1.36	−0.31	0.66	15.97	1.54
ΔG_{polar}	26.60	2.12	15.10	0.76	34.30	2.36
ΔH_{tot}	−140.99	12.97	−190.56	9.59	−221.43	11.94
-TΔS	36.19	16.18	39.94	14.43	44.34	16.08
ΔG_{tot} tot	**−104.80**		**−150.62**		**−177.09**	

[a] Standard deviation.

which depends on the initial orientation. This phenomenon was also supported by a previous MD research (Mücksch and Urbassek, 2011) of BSA adsorption on graphite surface.

Further insights into the driving forces involved in the adsorption can also be obtained by analyzing the free energies contributions (Table 3). In detail, the intermolecular van der Waals (ΔE_{vdw}) is important for the adsorption, whereas electrostatic interaction (ΔE_{ele}) has no contribution as the graphene is uncharged. The polar solvation terms (ΔG_{sol_polar}) are unfavorable, however, the non-polar solvation ones (ΔG_{sol_np}), which correspond to the burial of SASA upon binding, contribute favorably. As a result, both the polar interaction ($\Delta G_{polar} = \Delta E_{ele} + \Delta G_{sol\_polar}$) and the solvation contribution ($\Delta G_{sol} = \Delta G_{sol\_np} + \Delta G_{sol\_polar}$) are unfavorable for the adsorption in all orientations. Contrary to the contribution of the overall enthalpy, the overall entropic contribution is unfavorable. Hence, the binding free energy comes mainly from the nonpolar contributions, such as E_{vdw} and G_{sol_np}.

To further identify which parts of the protein are critical for PrP adsorption, the interaction energies between each residue of PrP (125–228) and the graphene surface are shown in Fig. 9. Consistent with the above results, the total enthalpy contribution of one residue is very close to its vdw contribution, indicating it interacts with graphene mainly by vdw interaction. The polar solvation terms (ΔG_{sol_polar}) are unfavorable. For Orientation 1, the hotspot residues (per residue contribution > 1 kcal mol^{-1}) are mainly distributed around the head of the three helices (H1, H2 and H3) and the loop near them; for Orientation 2, the hot spots locates mainly in the two β-sheets (S1 and S2) and the tail of H2 and H3; as for Orientation 3, the whole H3 helix is lying on the graphene as well as the residues near the head of H1 and H3. It is obvious that the hotspot residues are just those in contact with graphene.

4. Conclusions

In our present work, we investigated the atomic-level structural variations for $PrP_{125–228}$ on graphene surface to understand the effects of graphene on the structure of amyloid protein and further to explore

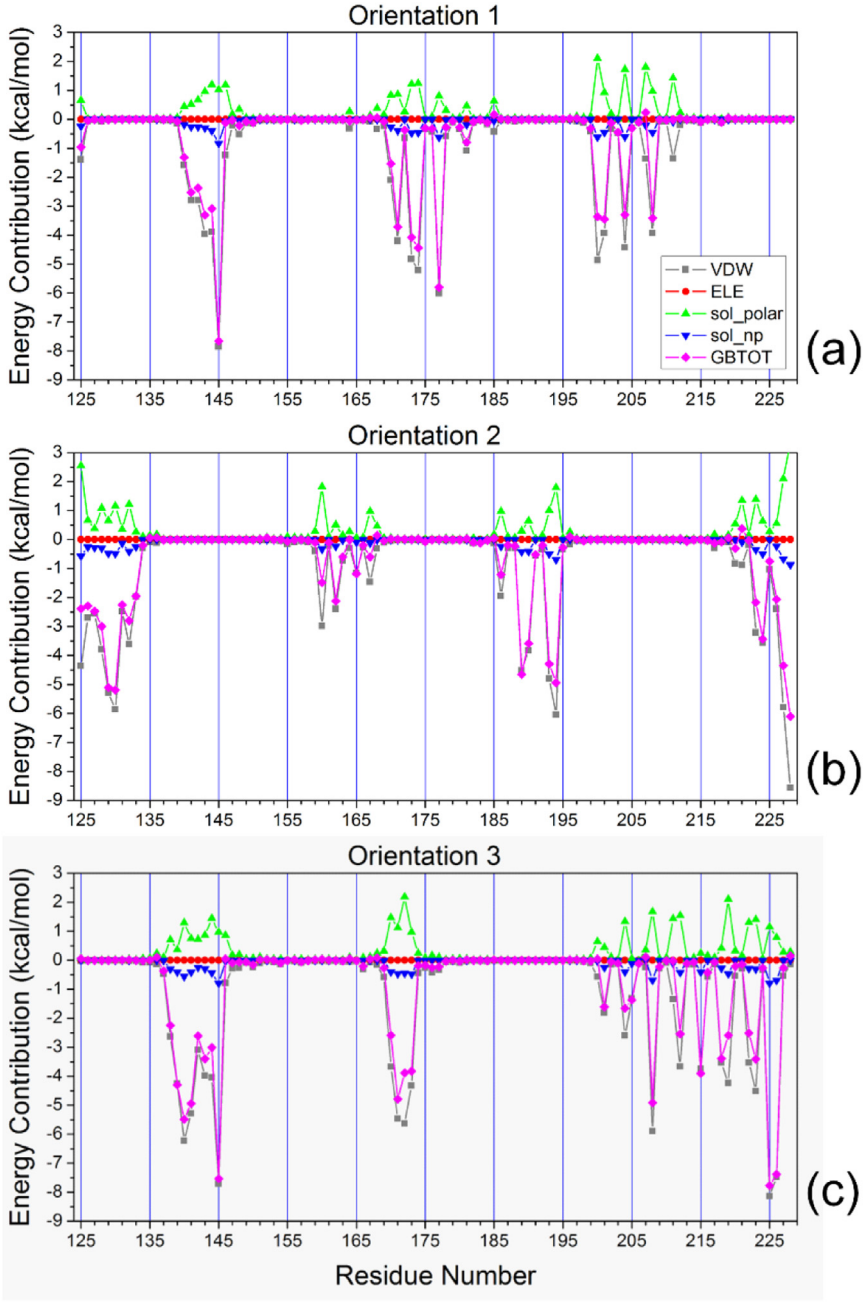

Fig. 9. The contribution of each residue calculated from MM-GBSA method.

the bio-safety of graphene in biomedical applications. The results from fluorescence quenching and circular dichroism spectrum experiments showed that the addition of graphene changed the secondary structure of global domain of prion largely and may strengthen the misfolding inclination of prion. The molecular dynamics simulations in explicit solvent suggest that the prion protein was quickly and tightly adsorbed onto the graphene sheet, and underwent a weak structural rearrangement progress. It was found that in adsorption runs the Rg of the hydrophobic core fluctuated rather wildly and were different from the isolated one, indicating the increased instability of hydrophobic core upon the absorption of prion on graphene. In more details, in adsorption runs, the helix contents decrease and the unstructured contents increase, indicating that the graphene can induce the partial misfolding of prion. The H1 region is the most instable part during the adsorption. Besides H1, the S2-H2 loop was found converting to a 3_{10}-helix or turn, which is related to the in vivo template-driven amplification of a prion and amyloid formation. On the contrary, the other regions are rather stable in the both adsorption runs and the isolated run. Hence the H1 and S2-H2 loop may play more important roles in the initial structural transition progress of PrP. Due that the carbon atoms of graphene have no charges, so the adsorption is mainly driven by vdw forces but not the polar interactions. Our work shows that graphene will induce the partial misfolding of prion protein. The obtained results can provide the detailed insights into the interaction of prion with graphene, which is valuable to the applications of graphene in biosystems and to understand the potential risk of graphene in the field of biomedicine.

Acknowledgements

This work was supported by the National Natural Science Foundation of China (Grant No: 21375054) and by the Fundamental Research Funds for the Central Universities (Grant No. lzujbky-2017-

k24).

References

Ashby, J., Pan, S., Zhong, W., 2014. Size and surface functionalization of iron oxide nanoparticles influence the composition and dynamic nature of their protein corona. ACS Appl. Mater. Interfaces 6, 15412–15419.

Balamurugan, K., Gopalakrishnan, R., Raman, S.S., Subramanian, V., 2010. Exploring the changes in the structure of α-helical peptides adsorbed onto a single walled carbon nanotube using classical molecular dynamics simulation. J. Phys. Chem. B 114, 14048–14058.

Balamurugan, K., Singam, E.R.A., Subramanian, V., 2011. Effect of curvature on the α-helix breaking tendency of carbon based nanomaterials. J. Phys. Chem. C 115, 8886–8892.

Baldrighi, M., Trusel, M., Tonini, R., Giordani, S., 2016. Carbon nanomaterials interfacing with neurons: an in vivo perspective. Front. Neurosci. 10, 250.

Berendsen, H.J.C., Postma, J.P.M., Van Gunsteren, W.F., DiNola, A., Haak, J.R., 1984. Molecular dynamics with coupling to an external bath. J. Chem. Phys. 81, 3684–3690.

Bianco, A., Kostarelos, K., Prato, M., 2008. Opportunities and challenges of carbon-based nanomaterials for cancer therapy. Expert Opin. Drug Deliv. 5, 331–342.

Bobylev, A., Marsagishvili, L., Podlubnaya, Z., 2010. Fluorescence analysis of the action of soluble derivatives of fullerene C60 on amyloid fibrils of the brain peptide Aβ(1–42). Biophysics 55, 699–702.

Brannon-Peppas, L., Blanchette, J.O., 2004. Nanoparticle and targeted systems for cancer therapy. Adv. Drug Deliv. Rev. 56, 1649–1659.

Calzolai, L., Zahn, R., 2003a. Influence of pH on NMR structure and stability of the human prion protein globular domain. J. Biol. Chem. 278, 35592–35596.

Calzolai, L., Zahn, R., 2003b. Influence of pH on NMR structure and stability of the human prion protein globular domain. J. Biol. Chem. 278, 35592–35596.

Case, D., Darden, T., Cheatham III, T., Simmerling, C., Wang, J., Duke, R., Luo, R., Crowley, M., Walker, R., Zhang, W., 2008. AMBER 10. University of California, San Francisco.

Cedervall, T., Lynch, I., Lindman, S., Berggård, T., Thulin, E., Nilsson, H., Dawson, K.A., Linse, S., 2007. Understanding the nanoparticle–protein corona using methods to quantify exchange rates and affinities of proteins for nanoparticles. Proc. Natl. Acad. Sci. USA 104, 2050–2055.

Chen, C., Dong, X.P., 2016. Epidemiological characteristics of human prion diseases. Infect. Dis. Poverty 5, 47.

Chen, M., Zeng, G., Xu, P., Yan, M., Xiong, W., Zhou, S., 2017. Interaction of carbon nanotubes with microbial enzymes: conformational transitions and potential toxicity. Environ. Sci.: Nano 4, 1954–1960.

Christen, B., Hornemann, S., Damberger, F.F., Wüthrich, K., 2009. Prion protein NMR structure from Tammar Wallaby (Macropus eugenii) Shows that the [beta]2-[alpha]2 loop is modulated by long-range sequence effects. J. Mol. Biol. 389, 833–845.

Conway, K.A., Harper, J.D., Lansbury, P.T., 1998. Accelerated in vitro fibril formation by a mutant α-synuclein linked to early-onset Parkinson disease. Nat. Med. 4, 1318–1320.

Dominguez-Medina, S., Kisley, L., Tauzin, L.J., Hoggard, A., Shuang, B., Indrasekara, D.S., Chen, A.S., Wang, S., Derry, L.-Y., Liopo, P.J., Liopo, A., Zubarev, E.R., Landes, C.F., Link, S., 2016. Adsorption and unfolding of a single protein triggers nanoparticle aggregation. ACS Nano 10, 2103–2112.

Donne, D.G., Viles, J.H., Groth, D., Mehlhorn, I., James, T.L., Cohen, F.E., Prusiner, S.B., Wright, P.E., Dyson, H.J., 1997. Structure of the recombinant full-length hamster prion protein PrP (29-C231): the N terminus is highly flexible. Proc. Natl. Acad. Sci. USA 94, 13452–13457.

Duan, Y., Wu, C., Chowdhury, S., Lee, M., Xiong, G., Zhang, W., Yang, R., Cieplak, P., Luo, R., Lee, T., 2003. A point-charge force field for molecular mechanics simulations of proteins based on condensed-phase quantum mechanical calculations. J. Comput. Chem. 24, 1999–2012.

Elsaesser, A., Howard, C.V., 2012. Toxicology of nanoparticles. Adv. Drug Deliv. Rev. 64, 129–137.

Essmann, U., Perera, L., Berkowitz, M.L., Darden, T., Lee, H., Pedersen, L.G., 1995. A smooth particle mesh Ewald method. J. Chem. Phys. 103, 8577–8593.

Fei, L., Perrett, S., 2009. Effect of nanoparticles on protein folding and fibrillogenesis. Int. J. Mol. Sci. 10, 646–655.

Feng, L., Liu, Z., 2011. Graphene in biomedicine: opportunities and challenges. Nanomedicine 6, 317–324.

Guo, J., Li, J., Zhang, Y., Jin, X., Liu, H., Yao, X., 2013. Exploring the influence of carbon nanoparticles on the formation of β-sheet-rich oligomers of $IAPP_{22-28}$ peptide by molecular dynamics simulation. PLoS One 8, e65579.

Guo, J.J., Ning, L.L., Ren, H., Liu, H.X., Yao, X.J., 2012a. Influence of the pathogenic mutations T188K/R/A on the structural stability and misfolding of human prion protein: insight from molecular dynamics simulations. Biochim. Biophys. Acta-Gen. Subj. 1820, 116–123.

Guo, J.J., Ren, H., Ning, L.L., Liu, H.X., Yao, X.J., 2012b. Exploring structural and thermodynamic stabilities of human prion protein pathogenic mutants D202N, E211Q and Q217R. J. Struct. Biol. 178, 225–232.

Gurunathan, S., Kim, J.H., 2016. Synthesis, toxicity, biocompatibility, and biomedical applications of graphene and graphene-related materials. Int. J. Nanomed. 11, 1927.

Hou, T., Wang, J., Li, Y., Wang, W., 2011a. Assessing the performance of the MM/PBSA and MM/GBSA methods. 1. The accuracy of binding free energy calculations based on molecular dynamics simulations. J. Chem. Inf. Model. 51, 69–82.

Hou, T., Wang, J., Li, Y., Wang, W., 2011b. Assessing the performance of the molecular mechanics/Poisson Boltzmann surface area and molecular mechanics/generalized Born surface area methods. II. The accuracy of ranking poses generated from docking. J. Comput. Chem. 32, 866–877.

Humphrey, W., Dalke, A., Schulten, K., 1996. VMD: visual molecular dynamics. J. Mol. Graph. 14, 33–38.

Jarosz, A., Skoda, M., Dudek, I., Szukiewicz, D., 2016. Oxidative stress and mitochondrial activation as the main mechanisms underlying graphene toxicity against human cancer cells. Oxid. Med. Cell. Longev. 2016, 5851035.

Jorgensen, W.L., Chandrasekhar, J., Madura, J.D., Impey, R.W., Klein, M.L., 1983. Comparison of simple potential functions for simulating liquid water. J. Chem. Phys. 79, 926–935.

Kabsch, W., Sander, C., 1983. Dictionary of protein secondary structure: pattern recognition of hydrogen-bonded and geometrical features. Biopolymers 22, 2577–2637.

Kaneko, K., Zulianello, L., Scott, M., Cooper, C.M., Wallace, A.C., James, T.L., Cohen, F.E., Prusiner, S.B., 1997. Evidence for protein X binding to a discontinuous epitope on the cellular prion protein during scrapie prion propagation. Proc. Natl. Acad. Sci. USA 94, 10069–10074.

Kelly, S.M., Jess, T.J., Price, N.C., 2005. How to study proteins by circular dichroism. Biochim. Biophys. Acta 1751, 119–139.

Kim, J.E., Lee, M., 2003. Fullerene inhibits β-amyloid peptide aggregation. Biochem. Biophys. Res. Commun. 303, 576–579.

Kollman, P.A., Massova, I., Reyes, C., Kuhn, B., Huo, S., Chong, L., Lee, M., Lee, T., Duan, Y., Wang, W., 2000. Calculating structures and free energies of complex molecules: combining molecular mechanics and continuum models. Acc. Chem. Res. 33, 889–897.

Kouassi, G.K., Wang, P., Sreevatan, S., Irudayaraj, J., 2007. Aptamer-mediated magnetic and gold-coated magnetic nanoparticles as detection assay for prion protein assessment. Biotechnol. Prog. 23, 1239–1244.

Kowalewski, T., Holtzman, D.M., 1999. In situ atomic force microscopy study of Alzheimer's β-amyloid peptide on different substrates: new insights into mechanism of β-sheet formation. Proc. Natl. Acad. Sci. USA 96, 3688–3693.

Lee, C.M., Huang, S.T., Huang, S.H., Lin, H.W., Tsai, H.P., Wu, J.Y., Lin, C.M., Chen, C.T., 2011. C60 fullerene-pentoxifylline dyad nanoparticles enhance autophagy to avoid cytotoxic effects caused by the β-amyloid peptide. Nanomed.: Nanotechnol. Biol. Med. 7, 107–114.

Lee, M., Duan, Y., 2004. Distinguish protein decoys by using a scoring function based on a new AMBER force field, short molecular dynamics simulations, and the generalized born solvent model. Protein.: Struct. Funct. Bioinform. 55, 620–634.

Li, H., Luo, Y., Derreumaux, P., Wei, G., 2011. Carbon nanotube inhibits the formation of β-sheet-rich oligomers of the Alzheimer's amyloid-β(16-22) peptide. Biophys. J. 101, 2267–2276.

Li, L., Zhu, Y., Zhou, S., An, X., Zhang, Y., Bai, Q., He, Y.X., Liu, H., Yao, X., 2017. Experimental and theoretical insights into the inhibition mechanism of prion fibrillation by resveratrol and its derivatives. ACS Chem. Neurosci. 8, 2698–2707.

Liang, L., Long, Y., Zhang, H., Wang, Q., Huang, X., Zhu, R., Teng, P., Wang, X., Zheng, H., 2013. Visual detection of prion protein based on color complementarity principle. Biosens. Bioelectron. 50, 14–18.

Linse, S., Cabaleiro-Lago, C., Xue, W.-F., Lynch, I., Lindman, S., Thulin, E., Radford, S.E., Dawson, K.A., 2007. Nucleation of protein fibrillation by nanoparticles. Proc. Natl. Acad. Sci. USA 104, 8691–8696.

Lou, Z., Wang, B., Guo, C., Wang, K., Zhang, H., Xu, B., 2015. Molecular-level insights of early-stage prion protein aggregation on mica and gold surface determined by AFM imaging and molecular simulation. Colloids Surf. B Biointerfaces 135, 371–378.

Lou, Z., Wan, J., Zhang, X., Zhang, H., Zhou, X., Cheng, S., Gu, N., 2017a. Quick and sensitive SPR detection of prion disease-associated isoform (PrP) based on its self-assembling behavior on bare gold film and specific interactions with aptamer-graphene oxide (AGO). Colloids Surf. B Biointerfaces 157, 31–39.

Lou, Z., Han, H., Zhou, M., Wan, J., Sun, Q., Zhou, X., Gu, N., 2017b. Fabrication of magnetic conjugation clusters via intermolecular assembling for ultrasensitive surface plasmon resonance (SPR) detection in a wide range of concentrations. Anal. Chem. 89, 13472–13479.

de Luna, L.A.V., de Moraes, A.C.M., Consonni, S.R., Pereira, C.D., Cadore, S., Giorgio, S., Alves, O.L., 2016. Comparative in vitro toxicity of a graphene oxide-silver nanocomposite and the pristine counterparts toward macrophages. J. Nanobiotechnol. 14, 12.

Mahmoudi, M., Lynch, I., Ejtehadi, M.R., Monopoli, M.P., Bombelli, F.B., Laurent, S., 2011. Protein–nanoparticle interactions: opportunities and challenges. Chem. Rev. 111, 5610–5637.

Mahmoudi, M., Akhavan, O., Ghavami, M., Rezaee, F., Ghiasi, S.M.A., 2012. Graphene oxide strongly inhibits amyloid beta fibrillation. Nanoscale 4, 7322–7325.

Matsuo, K., Sakurada, Y., Tate, S., Namatame, H., Taniguchi, M., Gekko, K., 2012. Secondary-structure analysis of alcohol-denatured proteins by vacuum-ultraviolet circular dichroism spectroscopy. Proteins 80, 281–293.

Matsuo, K., Maki, Y., Namatame, H., Taniguchi, M., Gekko, K., 2016. Conformation of membrane–bound proteins revealed by vacuum–ultraviolet circular–dichroism and linear-dichroism spectroscopy. Protein.: Struct. Funct. Bioinform. 84, 349–359.

Meli, M., Gasset, M., Colombo, G., 2011. Dynamic diagnosis of familial prion diseases supports the β2-α2 loop as a universal interference target. PLoS One 6, e19093.

Mendes, R.G., Bachmatiuk, A., Buchner, B., Cuniberti, G., Rummeli, M.H., 2013. Carbon nanostructures as multi-functional drug delivery platforms. J. Mater. Chem. B 1, 401–428.

Merli, D., Ugonino, M., Profumo, A., Fagnoni, M., Quartarone, E., Mustarelli, P., Visai, L., Grandi, M.S., Galinetto, P., Canton, P., 2011. Increasing the antibacterial effect of lysozyme by immobilization on multi-walled carbon nanotubes. J. Nanosci. Nanotechnol. 11, 3100–3106.

Mücksch, C., Urbassek, H.M., 2011. Molecular dynamics simulation of free and forced

BSA adsorption on a hydrophobic graphite surface. Langmuir 27, 12938–12943.
Podlubnaya, Z., Podol'skii, I., Shpagina, M., Marsagishvili, L., 2006. Electron microscopic study of the effect of fullerene on the formation of amyloid fibrils by the Aβ25–35 peptide. Biophysics 51, 701–704.
Prusiner, S.B., McKinley, M.P., Bowman, K.A., Bolton, D.C., Bendheim, P.E., Groth, D.F., Glenner, G.G., 1983. Scrapie prions aggregate to form amyloid-like birefringent rods. Cell 35, 349–358.
Riek, R., Hornemann, S., Wider, G., Billeter, M., Glockshuber, R., Wüthrich, K., 1996. NMR structure of the mouse prion protein domain PrP (121-231). Nature 382, 180–182.
Ryckaert, J.P., Ciccotti, G., Berendsen, H.J.C., 1977. Numerical integration of the Cartesian equations of motion of a system with constraints: molecular dynamics of n-alkanes. J. Comput. Phys. 23, 327–341.
Sanchez, V.C., Jachak, A., Hurt, R.H., Kane, A.B., 2011. Biological interactions of graphene-family nanomaterials: an interdisciplinary review. Chem. Res. Toxicol. 25, 15–34.
Sharifi, S., Behzadi, S., Laurent, S., Laird Forrest, M., Stroeve, P., Mahmoudi, M., 2012. Toxicity of nanomaterials. Chem. Soc. Rev. 41, 2323–2343.
Shen, H., Zhang, L., Liu, M., Zhang, Z., 2012. Biomedical applications of graphene. Theranostics 2, 283–294.
Srinivasan, J., Cheatham III, T.E., Cieplak, P., Kollman, P.A., Case, D.A., 1998. Continuum solvent studies of the stability of DNA, RNA, and phosphoramidate- DNA helices. J. Am. Chem. Soc. 120, 9401–9409.
Sun, B., Wang, M., Lou, Z., Huang, M., Xu, C., Li, X., Chen, L.J., Yu, Y., Davis, G.L., Xu, B., Yang, H.B., Li, X., 2015. From ring-in-ring to sphere-in-sphere: self-assembly of discrete 2D and 3D architectures with increasing stability. J. Am. Chem. Soc. 137, 1556–1564.
Tenzer, S., Docter, D., Rosfa, S., Wlodarski, A., Kuharev, J., Rekik, A., Knauer, S.K., Bantz, C., Nawroth, T., Bier, C., Sirirattanapan, J., Mann, W., Treuel, L., Zellner, R., Maskos, M., Schild, H., Stauber, R.H., 2011. Nanoparticle size is a critical physicochemical determinant of the human blood plasma corona: a comprehensive quantitative proteomic analysis. ACS Nano 5, 7155–7167.
Wang, B., Guo, C., Lou, Z., Xu, B., 2015. Following the aggregation of human prion protein on Au(111) surface in real-time. Chem. Commun. 51, 2088.
Wei, T., Carignano, M.A., Szleifer, I., 2012. Molecular dynamics simulation of lysozyme adsorption/desorption on hydrophobic surfaces. J. Phys. Chem. B 116, 10189–10194.
Yu, X., Wang, Q., Lin, Y., Zhao, J., Zhao, C., Zheng, J., 2012. Structure, orientation, and surface interaction of alzheimer amyloid-β peptides on the graphite. Langmuir 28, 6595–6605.
Zhang, L.Y., Zheng, H.Z., Long, Y.J., Huang, C.Z., Hao, J.Y., Zhou, D.B., 2011. CdTe quantum dots as a highly selective probe for prion protein detection: colorimetric qualitative, semi-quantitative and quantitative detection. Talanta 83, 1716–1720.
Zhang, Y., Nayak, T.R., Hong, H., Cai, W., 2012. Graphene: a versatile nanoplatform for biomedical applications. Nanoscale 4, 3833–3842.
Zhou, J., Zheng, J., Jiang, S., 2004. Molecular simulation studies of the orientation and conformation of cytochrome c adsorbed on self-assembled monolayers. J. Phys. Chem. B 108, 17418–17424.
Zhou, S., Liu, X., An, X., Yao, X., Liu, H., 2017. Molecular dynamics simulation study on the binding and stabilization mechanism of antiprion compounds to the "hot spot" region of PrP. ACS Chem. Neurosci. 8, 2446–2456.